IEEE Photonics Journal
An IEEE Photonics Society Publication

D-Band mm-Wave SSB Vector Signal Generation Based on Cascaded Intensity Modulators

Volume 12, Number 2, April 2020

Yitong Li
You-Wei Chen
Wen Zhou
Xizi Tang
Jin Shi
Li Zhao
Jianguo Yu
Gee-Kung Chang

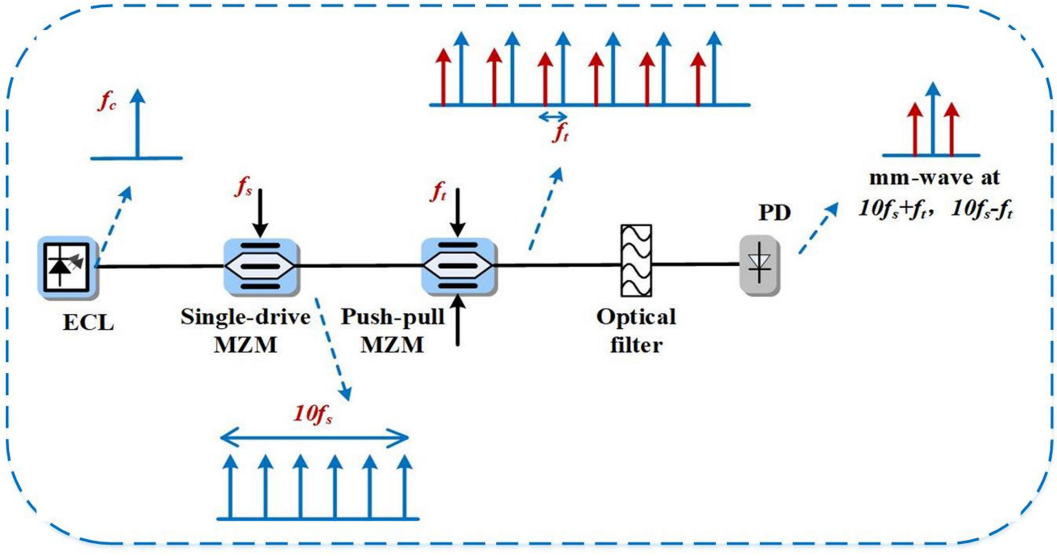

DOI: 10.1109/JPHOT.2020.2974256

D-Band mm-Wave SSB Vector Signal Generation Based on Cascaded Intensity Modulators

Yitong Li,[1,2] **You-Wei Chen**,[2] **Wen Zhou**,[2] **Xizi Tang**,[1,2] **Jin Shi**,[2] **Li Zhao**,[2] **Jianguo Yu**,[1] **and Gee-Kung Chang**[2]

[1]School of Electronic Engineering, Beijing University of Posts and Telecommunications, Beijing 100876, China
[2]School of Electrical and Computer Engineering, Georgia Institute of Technology, Atlanta 30308 Georgia USA

DOI:10.1109/JPHOT.2020.2974256

Manuscript received December 27, 2019; revised February 4, 2020; accepted February 11, 2020. Date of publication February 17, 2020; date of current version March 26, 2020. This work was supported in part by the National Natural Science Foundation of China, under Grant 61821001 and in part by the China Scholarship Council CSC, under Grant 201806470039. Corresponding author: Jianguo Yu (email: yujg@bupt.edu.cn).

Abstract: We proposed and experimentally demonstrated a novel and simple method to realize D-band millimeter-wave (mm-wave) single-sideband (SSB) vector signal generation using cascaded one single-drive Mach-Zehnder modulator (MZM) and one push-pull MZM. After the first MZM driven by a radio frequency (RF) signal of 20-GHz, an optical frequency comb (OFC) with six flat carriers was successfully generated. Using the subsequent push-pull MZM driven by 10-GHz SSB vector signals and a photodiode (PD) for detection, we finally generated D-band SSB vector mm-wave signals at frequencies of 130-GHz and 150-GHz, respectively. The experimental results are well consistent with theoretical and simulation analysis. Based on the proposed scheme, 4-Gbaud generated D-band quadrature phase shift keying (QPSK) and 16 quadrature amplitude modulation (16QAM) mm-wave signals were transmitted over 10-km/25-km single-mode-fiber (SMF) and 1-m wireless links. The bit-error-rate (BER) performance can reach less than 7% hard-decision forward-error-correction (FEC) threshold of 3.8×10^{-3}.

Index Terms: Optical frequency comb, single-sideband modulation, intensity modulator, radio-over-fiber and millimeter-wave generation.

1. Introduction

Radio-over-fiber (ROF) is a technology for radio access networks that integrates fiber optics and wireless data transmission in order to fulfill the tremendous demand for high-speed and large-capacity wireless applications. As a key technology in ROF systems, millimeter-wave (mm-wave) signal (30 GHz–300 GHz) generation has been widely investigated because mm-wave has abundant bandwidth and it can achieve a high transmission rate [1]–[4]. The most commonly used method for mm-wave generation is based on external optical modulator including single modulator [5], [6] and multiple cascaded modulators [7], [8], since the generated mm-wave base on this kind of method has high-stability and high-purity. Nowadays, a lot of research on W-band mm-wave (75 GHz–110 GHz) generation has been proposed [9]–[12]. Compared to W-band mm-wave, D-band (110 GHz–170 GHz) has higher frequency and wider bandwidth which can provide higher

transmission rate as well as lower atmospheric and rain attenuation [13]–[15]. The D-band mm-wave generation technology can not only solve the problem of high-capacity mobile data access to the Internet and high-speed wireless transmission between smart devices, but also be used in deep space communications as well as emergency communications. Therefore, generating D-band mm-waves at high frequencies is desired and it is also the trend for future communication systems.

To generate mm-wave vector modulated signals, different modulation schemes have been demonstrated including optical carrier suppression (OCS) [16], [17], double-sideband (DSB) [18] and single-sideband (SSB) [19]–[22]. In stark contrast to DSB modulation, SSB can reduce the impairment caused by fiber dispersion and extend the transmission distance over single-mode-fiber (SMF) [20], as well as the bandwidth efficiency is double as compared of DSB. Besides, by applying SSB modulation, the required wavelength interval can be reduced and consequently the wavelength numbers in dense wavelength-division-multiplexing (WDM) systems can be increased for enlarging the channel.

Moreover, to improve the flexibility and solve the problem of frequency overlay in ROF system, mm-wave signal generation based on optical frequency comb has been widely employed. The system with frequency multiplication modulation such us the tripling [22], quadrupling [23], sex-tupling [24] and even octupling [9], [11] frequency schemes for mm-wave generation have been reported. However, these schemes have inevitably adopted complex transmitter precoding process which not only complicates the experiment operation, but also reduces the Euclidean distance of transmitter constellation and therefore decreases the capacity and delivery distance thus resulting in the system performance deterioration.

Based on the above analysis, in this paper, we proposed a novel scheme to generate vector D-band mm-wave signals without the transmitter precoding. By employing two cascaded intensity modulators both optical frequency combs and SSB modulation were conducted. We firstly theoretically analyzed the principle of comb generation and SSB modulation process and then show the obtained simulation results of comb generation using VPI software. Furthermore, we experimentally applied a radio frequency (RF) driving signal of 20-GHz on the first Mach-Zehnder modulator (MZM) to generate multi-tones and six flat odd-order-carriers (namely ±1, ±3, ±5 order sidebands) are finally generated with a frequency spacing of 40-GHz after an even-order-carriers (namely 0, ±2, ±4 order sidebands) suppression process. Multiple frequencies of mm-wave can be easily generated by selecting any two arbitrary carriers among the reserved carriers for beating with SSB vector signals at the frequency of 10-GHz. For the purpose of performance analysis, we selected -5, $+3$ and -3, $+3$ orders sidebands respectively to beat with the SSB signals. 130-GHz 4-Gbaud and 150-GHz 4-Gbaud D-band mm-waves with QPSK/16QAM information are generated and transmitted over 10-km/25-km SMF and 1-m wireless link in our experiment. To best of our knowledge, it is the first time to realize the D-band vector mm-wave generation with optical combs and SSB modulation using cascaded intensity modulators. This is a promising technology for ROF systems in 5th-generation (5G) and even next-generation communication, since it simplifies DSP process of the transmitter end, increases the flexibility of mm-wave frequencies generation and boosts the bandwidth as well as the transmission rate.

2. Theoretical Analysis and Simulations

2.1 Principle for Optical Frequency Comb Generation Based on the First Intensity Modulator

Figure 1 shows the principle of optical frequency comb generation based on an external cavity laser (ECL) cascaded by an intensity modulator. The output optical field from the ECL can be expressed as

$$E_{ECL}(t) = E_0 \cdot \exp(j2\pi f_c t) \tag{1}$$

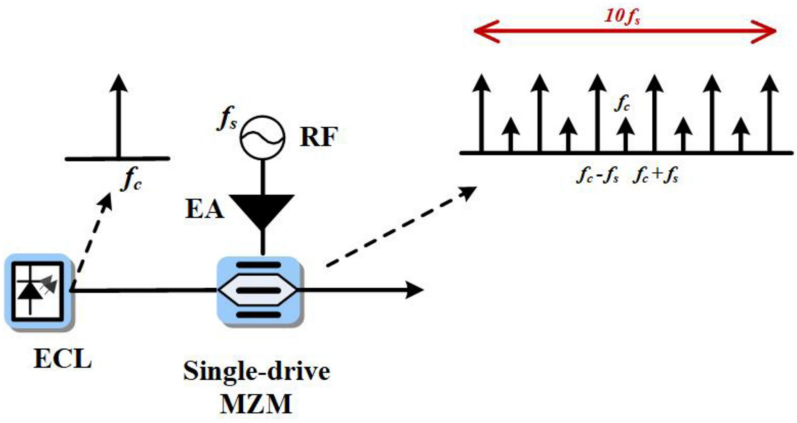

Fig. 1. Scheme for optical frequency comb generation based on one MZM. ECL: external cavity laser. RF: radio frequency. EA: electric amplifier. MZM: Mach-Zehnder modulator.

where E_0 represents the constant optical amplitude and f_c means the central frequency of the output lightwave of ECL. The RF driving signal for the subsequent MZM is expressed as

$$V_{drive}(t) = V_{RF} \cdot \cos 2\pi f_s t \tag{2}$$

where V_{RF} and f_s represent the driving voltage and frequency, respectively. The RF driving signal is amplified by an electric amplifier (EA) and used to drive a single-drive MZM. The optical field output of this single-drive MZM can be expressed as

$$\begin{aligned} E_{out}(t) &= \frac{1}{2} E_{ECL}(t)\left[\exp\left(j\pi\frac{V_{drive}+V_{DC}}{2}\right)+\exp\left(-j\pi\frac{V_{drive}+V_{DC}}{V_\pi}\right)\right] \\ &= E_{ECL}(t)\cos\left(\pi\frac{V_{drive}}{V_\pi}+\pi\frac{V_{DC}}{V_\pi}\right) \\ &= E_0 \exp(2\pi f_c t)\cos\left(\pi\frac{V_{RF}\cdot\cos 2\pi f_s t}{V_\pi}+\pi\frac{V_{DC}}{V_\pi}\right) \end{aligned} \tag{3}$$

where V_{DC} represents direct current (DC) bias applied on MZM, V_π denotes half-wave voltage of the MZM. Using the Jacobi-Anger identity:

$$e^{jx\cos\theta} = \sum_{n=-\infty}^{\infty} j^n J_n(x)\, e^{jn\theta} \tag{4}$$

to expand the $E_{out}(t)$ into the first kind Bessel function [16], we can obtain the formula as

$$\begin{aligned} E_{out}(t) = E_0 \cos\varphi \sum_{n=-\infty}^{\infty} (-1)^n J_{2n}(\beta)\exp(j2\pi f_c t + j2n\cdot 2\pi f_s t) \\ - E_1 \sin\varphi \sum_{n=-\infty}^{\infty} (-1)^n J_{2n+1}(\beta)\exp[j2\pi f_c t + j(2n+1)\cdot 2\pi f_s t] \end{aligned} \tag{5}$$

where $J_n(\beta)$ denotes the Bessel function of the first kind, and it is defined as:

$$J_n(x) = \sum_{m=0}^{\infty} (-1)^m \frac{x^{n+2m}}{2^{n+2m} m!\Gamma(-n+m+1)}, (n \geq 0) \tag{6}$$

$\varphi = \frac{\pi V_{DC}}{V_\pi}$ represents the initial phase caused by the DC bias voltage of MZM, and $\beta = \frac{\pi V_{RF}}{V_\pi}$ represents the modulation depth.

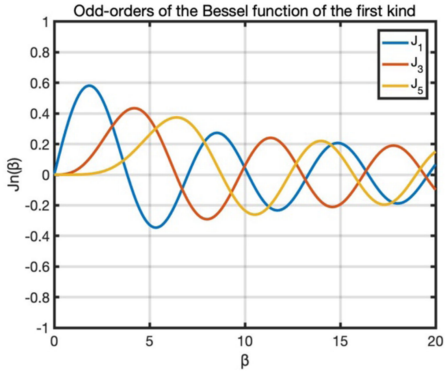

Fig. 2. Diagram for odd-orders of the Bessel function of the first kind.

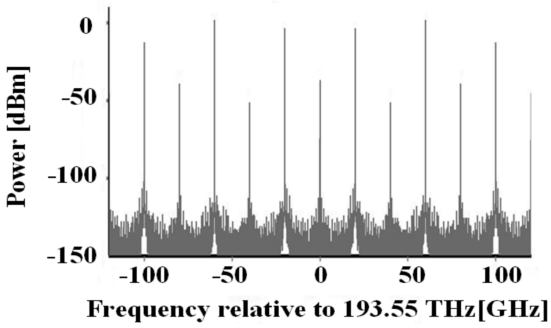

Fig. 3. Spectrum of simulation results for OFC generation based one single-drive MZM.

According to Eq. (5), the frequency components include the central frequency of f_c, the first-order-sidebands frequencies of $f_c \pm f_s$, the second-order-sidebands frequencies of $f_c \pm 2f_s$ and so on. The frequency spacing between each adjacent sideband is equal to the frequency, i.e., f_s of the RF driving signal. The amplitude of each sideband depends on the first Bessel function value $J_n(\beta)$ of each sideband as well as the initial phase variation caused by the DC bias voltage. When we control the DC bias of MZM properly and make $V_{DC} = V_\pi/2$, which means $\varphi = \pi/2$, Eq. (5) can be simplified to

$$E_{out}(t) = -E_0 \sum_{n=-\infty}^{\infty} (-1)^n J_{2n+1}(\beta) \exp\left[j2\pi f_c t + j(2n+1)2\pi f_s t\right] \tag{7}$$

In this case, odd-order-sidebands of the optical signal are preserved while even-order-sidebands including the center carrier are suppressed. Fig. 2 illustrates the Bessel function of the first kind for the first-order, third-order and fifth-order. We can see that as the order of sideband increases, its power peak decreases. By adjusting the voltage of the RF driving, we can change the power of the obtained frequency comb. When changing the DC bias voltage appropriately, we can obtain a comb that has flattop odd-order-sidebands and power suppressed even-order-sidebands. The frequency spacing of the reserved odd-order-sidebands is $2f_s$. Fig. 3 shows an obtained comb spectrum using VPI software simulation based on a single-drive MZM.

2.2 Principle for SSB Modulation Based on One Push-Pull MZM

As we know, optical SSB signals can be generated based on an IQ modulator [25], [26]. Compared with the conventional IQ modulators, the push-pull modulator has the advantages of lower cost, simpler structure and easier implementation. Fig. 4 shows the scheme for SSB signal generation

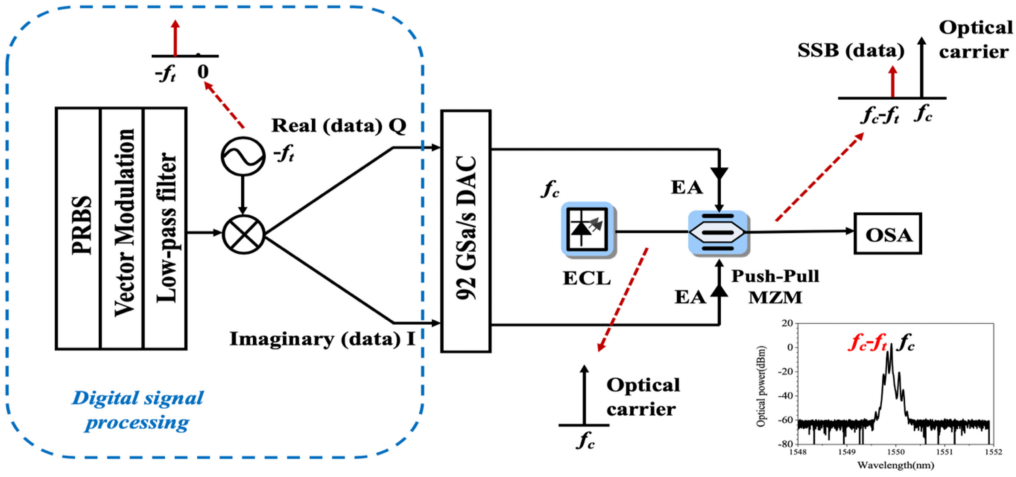

Fig. 4. Scheme for the generation of the SSB signal based on one push-pull modulator, the inset is the spectrum after push-pull modulator when no modulation on single-drive MZM in the experiment.

based on a dual-drive MZM, the inset is the spectrum after push-pull modulator when we only employ one push-pull MZM and no modulation on the single-drive MZM in the experiment. The push-pull MZM is constituted by two PMs which are regarded as its two arms. By adjusting the difference between the DC bias voltages on the two arms and simultaneously controlling the difference between input RF signals on each arm, the push-pull MZM can work in SSB modulation mode. The two arms normally have a different DC bias with a phase shift of $(2k+1)\pi/2$, where k is integer, while the different RF signals of each arm are with a phase shift of $\pm\pi/2$, thus SSB modulation can be realized. The driving vector signal at a frequency of f_t is generated by MATLAB-based offline DSP and applied on the push-pull MZM. A digital-to-analog converter (DAC) converts the digital vector signal prior to launching it into the MZM for the SSB signal generation. The driving electrical SSB signal can be expressed as

$$E_{data} = A\exp(-j2\pi f_t t) \tag{8}$$

where f_t denotes the driving carrier frequency of the RF signal, which is 10 GHz in our experiment. A means the data with different modulation formats. Varieties of modulation formats including single-carrier signals (QPSK and QAM, etc.) and orthogonal-frequency-division-multiplexing (OFDM) can be applied to modulate the RF driving signals. In our experiment, we operate single-carrier QPSK and 16QAM modulation, respectively, as a proof-of-concept demonstration. Assuming the continuous-wavelength (CW) lightwave from ECL is at the frequency of f_c and we apply it to modulate the RF SSB signal f_t via the push-pull MZM. The optical output for the push-pull MZM can be expressed as

$$E_{push-pull\ MZM} = [\alpha A exp(-j2\pi f_t t) + \gamma]\ \ \exp(j2\pi f_c t) = \alpha A exp[j2\pi (f_c - f_t) t] + \gamma exp(j2\pi f_c t) \tag{9}$$

where α denotes the response of the push-pull MZM and γ means the DC component of the frequency of optical carrier. The DC bias of two arms (the real and imaginary components) of the MZM is set at quadrature point. The SSB signals is generated by driving the push-pull modulator at a bias of $0.5V_\pi$ for its real and imaginary parts.

2.3 Proposed Scheme for MMW Generation

In our experiment, we cascaded the single-drive MZM and push-pull MZM. The optical comb and SSB modulation are both realized for mm-wave vector signal generation with flexible frequency selectivity after heterodyne beating through a photodiode (PD) with a bandwidth of 60 GHz in

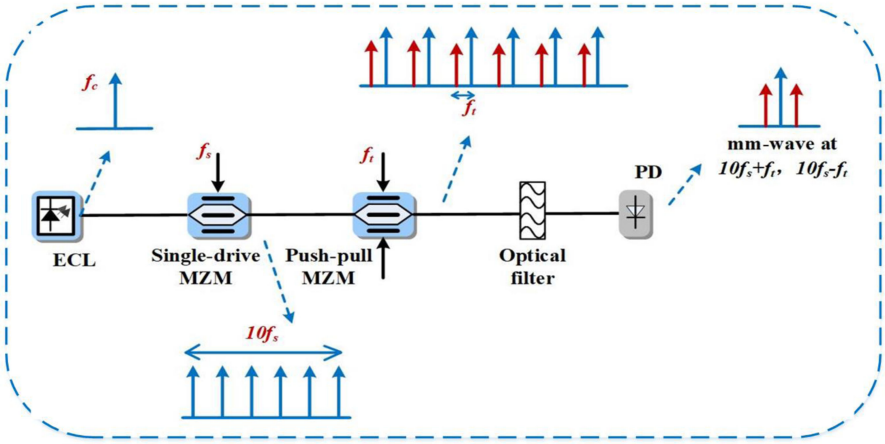

Fig. 5. Mm-wave vector signal generation based on two cascaded MZMs.

this system. Fig. 5 shows a conceptual diagram for a theoretical model of vector mm-wave signal generation by our proposed structure. Firstly, the CW is transmitted by an ECL and passes through one single-drive MZM. An optical frequency comb can be generated with even-order-sidebands suppression by setting a proper DC bias for the single-drive MZM. Odd-order-sidebands go through a push-pull MZM and are modulated by the push-pull MZM for optical SSB signal generation. The frequency spacing of the obtained SSB-modulated signal is determined by the frequency of the RF driving of the push-pull MZM. After that, using an optical filter and PD, we can select any two carriers with SSB signals to beat and generate frequency multiplication mm-wave signals based on SSB modulation.

3. Experimental Setup and Results

Figure 6 depicts our experimental setup of the ROF system for D-band 130 GHz/ 150 GHz mm-wave generation and transmission based on the proposed scheme. A CW is generated by an ECL at a central wavelength of 1550 nm with less than 100-kHz linewidth and 13-dBm output power and modulated by a single-drive MZM with a 20-GHz RF driving signal. The half-wave voltage of the first single-drive MZM is 2.7 V at 1 GHz and the 3-dB bandwidth is 37 GHz. The RF driving voltage on the MZM is 21 V_{pp} (V_{pp} is the peak to peak voltage). By changing the DC bias of the first MZM properly, we obtain a comb that has six odd-order-carriers with good flatness, as shown in Fig. 6(a) at 0.02-nm resolution. The reserved carriers are $\pm$1st, $\pm$3rd, $\pm$5th order sidebands which have a frequency spacing of 20-GHz. Even-order and undesired sidebands are all suppressed in this process, which reduces the number of tones into a subsequent polarization-maintaining erbium-doped fiber amplifier (PM-EDFA) and increases the power efficiency in the PM-EDFA amplification process. The PM-EDFA is used to amplify the output optical power of the first single-drive MZM because the MZM inevitably causes insertion and modulation loss to the scheme. After that, we employ another two-arm push-pull MZM with a 3-dB bandwidth of 35 GHz and a half-wave voltage of 2.7 V at 1 GHz. The DC bias of this push-pull MZM is set at quadrature point. QPSK/16QAM data are vector-modulated and generated in the transmitter DSP process. After mixing with the driving signal at a frequency of -10 GHz, the vector digital signals can be linearly converted to SSB signals which is located at -10 GHz in digital domain, as illustrated in Fig. 4. We add up the real and imaginary part of the SSB vector signal digitally to construct data I and data Q. And a 92-GSa/s DAC is used to convert digital data I and Q to analog signals. After the amplification process by EAs, the data I and Q can be used to drive the push-pull MZM to achieve the SSB modulation. Thus, an optical frequency comb with SSB modulation can be generated, as shown in Fig. 6(b).

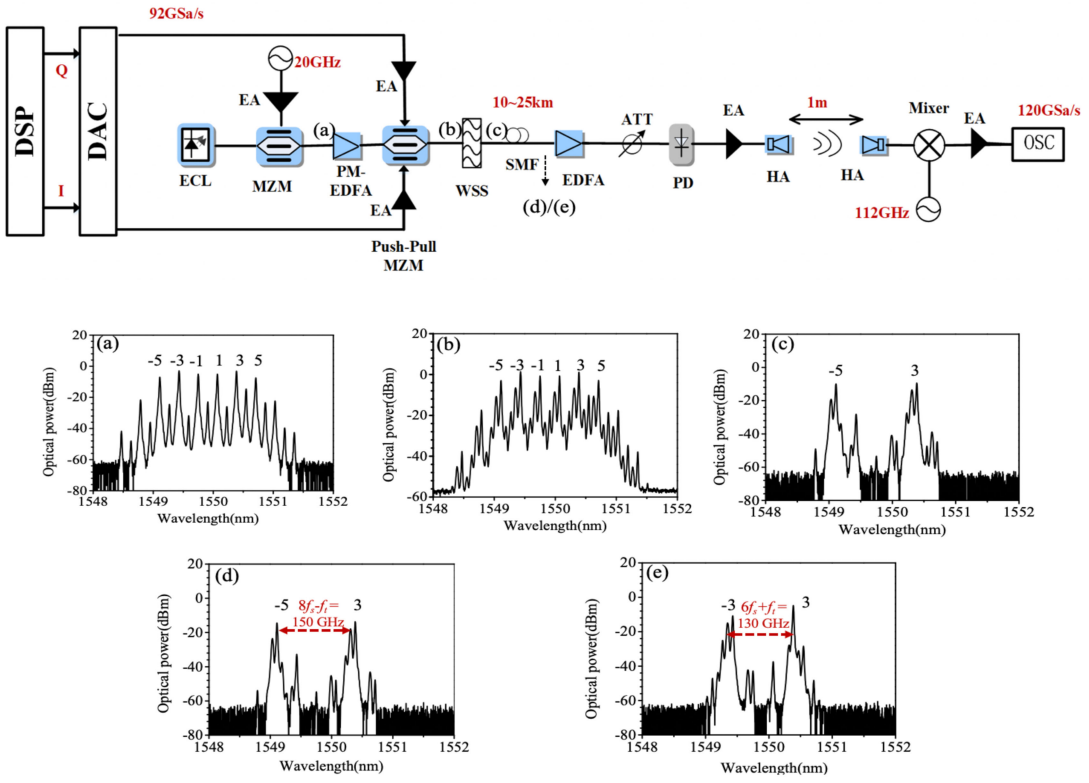

Fig. 6. Experimental setup of ROF system for D-band QPSK/16QAM mm-wave generation and transmission. Optical spectra (0.02 nm resolution): (a) after the first MZM (b) after push-pull MZM (c) after WSS (150 GHz mm-wave) (d) after 25-km SMF (150 GHz mm-wave) (e)after 25-km SMF (130 GHz mm-wave). ECL: external cavity laser; MZM: Mach-Zehnder modulator; PM-EDFA: polarization-maintaining erbium-doped fiber amplifier; WSS: wavelength selector switch; SMF: single-mode fiber; EA: electric amplifier; ATT: optical attenuator; PD: photodiode; HA: horn antenna; OSC: oscilloscope.

In the experiment, the -5th and $+3$rd order sidebands of the comb are selected firstly by a wavelength selector switch (WSS). Next, the two reserved optical QPSK/16QAM-modulated carriers are transmitted over 10-km/25-km SMF. After an EDFA amplification and an optical attenuator (ATT), the two sidebands with a frequency spacing of 160 GHz (i.e., $8f_s$) beat with the -10-GHz (i.e., $-f_t$) SSB vector signal and 150-GHz (i.e., $8f_s - f_t$) mm-wave signal can be generated through a D-band single-ended PD. An EA with 30-dB gain and DC$\sim$50-GHz operating range is used to boost the 150-GHz mm-wave before the 1-m wireless link transmission by two D-band horn antennas (HAs) with 25-dBi gain. Then after using the mixer with a 112-GH driving local oscillator (LO), the final intermediate frequency (IF) signal that we observe on real time digital oscilloscope (OSC) with 45-GHz electrical bandwidth and 120-GSa/s sampling rate is 38 GHz. Actually, another mm-wave signal at a frequency of 170-GHz (i.e., $8f_s + f_t$) is also generated. However, after a down-convert process by a mixer with LO at a frequency of 112-GHz, the actual frequency we obtain is 58 GHz, which is too high to be detected by our OSC with 45 GHz electrical bandwidth. So, we only detected the 150-GHz mm-wave signal. At the receiving side, the QPSK/16QAM data at the 150-GHz vector mm-wave signal is sampled and then processed offline DSP to compensate the accumulated dispersion.

Using our scheme, multi-frequency and multi-band mm-wave signals can be generated. The highest frequency that can be generated is 210 GHz (i.e., $10f_s + f_t$) by selecting -5 and $+5$ order sidebands of the generated comb. In the same way, we then generate and delivery a 130-GHz 16QAM D-band mm-wave to verify the flexibility for different frequencies generation by

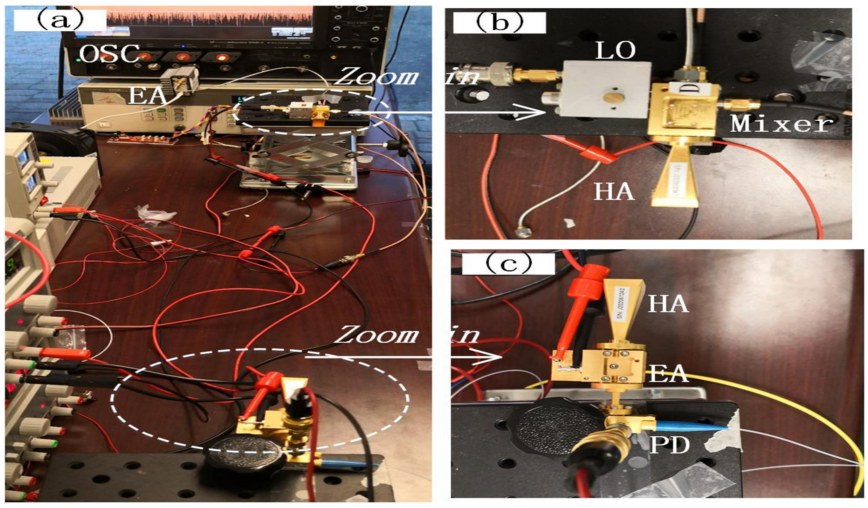

Fig. 7. (a) Whole wireless link system; (b) D-band wireless receiving side; (c) D-band wireless transmitting side.

selecting the -3rd and +3rd order sidebands. And after beating them with the 10-GHz SSB signal, we generate a 130-GHz (i.e., $6f_s + f_t$) D-band vector mm-wave signal. After the down-conversion process by LO at a frequency of 112-GHz, we finally observe an IF signal of 18-GHz using the OSC. In fact, 110-GHz (i.e., $6f_s - f_t$) mm-wave is also generated, the captured signal frequency at OSC of which is 2 GHz after mixing with the LO. The spectrum of this signal at 2 GHz is spectrally separated and will not influence the desired signal at 18 GHz. Figs. 6(c) and 6(d) give the optical spectra of the reserved carriers for generating a 150-GHz signal after WSS as well as after 25-km SMF, respectively. Fig. 6(e) shows the optical spectrum of the reserved sidebands for generating a 130-GHz signal after 25-km SMF. The experimental scenes are shown in Figs. 7(a–c).

Fig. 8(a) illustrates the BER performances of 150-GHz 4-Gbaud QPSK mm-wave signal in three situations: (1) 1-m wireless transmission only; (2) 1-m wireless and 25-km SMF optical transmission; (3) 1-m wireless and 10-km SMF optical delivery scheme. The experimental results show that when we increase the input power into PD, the measured BER performance of 150-GHz 4-Gbaud QPSK mm-wave signal will be improved due to larger SNR. The BER in all the three situations can reach under the hard-decision forward-error-correction (HD-FEC) threshold of 3.8×10^{-3}. The BER curves of the 1-m wireless and back-to-back delivery (situation 1, marked by black squares) and 1-m wireless and 10-km wired transmission (situation 2, marked by blue triangles) are very similar. Both cases can reach the HD-FEC when the input power into PD is -5.5 dBm. One can note that the BER performance is obviously deteriorated when the SMF transmission distance is increased to 25 km (situation 3, marked by red circles). There is a 1.5-dBm power penalty after 25-km SMF delivery due to chromatic dispersion. When the input power is -2.5 dBm, the BER performance in situation 3 reaches the best BER performance of 1×10^{-4}. Fig. 8(b) i-v illustrates the recovered constellation of 150-GH 4-Gbaud QPSK signal over 1-m wireless link after digital signal processing (DSP) technologies including down conversion, resampling, constant-modulus-algorithm (CMA), frequency offset estimation (FOE) and phase offset estimation (POE) [27]–[31]. Through this process, the constellation diagram change from an unclear pie in Fig. 8(b)–i into 4 clear QPSK constellation points in Fig. 8(b)–v. Electrical spectrum of the received 38-GHz IF signal after a down-conversion mixer is illustrated in Fig. 8(c).

To further increase the achievable capacity, the 150-GHz 16QAM vector mm-wave signal is also adopted for transmission. Fig. 9(a) shows the BER curves of 150-GHz 4-Gbaud 16QAM signal over 1-m wireless and 0-km/10-km fiber link. Again, two cases have similar BER performance. We measure the BER starting from the input power into PD of -2.5 dBm at an interval of 1 dBm. A total

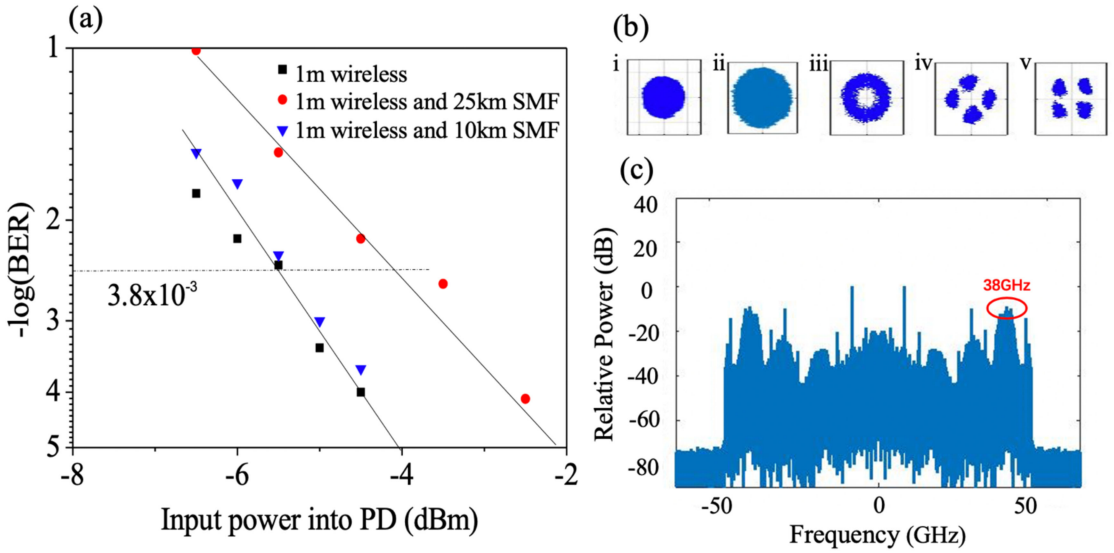

Fig. 8. Experimental results of the 150-GHz 4-Gbaud QPSK signal. (a) BER curves versus received power of PD; (b) the recovered constellation in 1-m wireless transmission case using DSP technology at 1.5-dBm input power in PD: (b)-i after down conversion; (b)-ii after resampling; (b)-iii after CMA; (b)-iv after FOE; (b)-v after POE. (c) the electrical spectrum of the IF signal at 38-GHz captured by OSC.

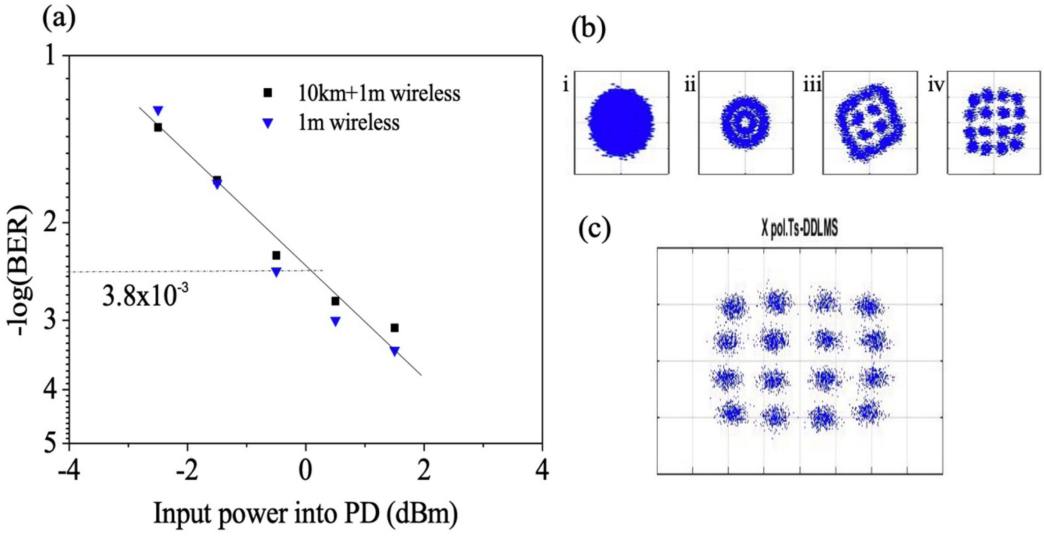

Fig. 9. Experimental results of 150-GHz 4-Gbaud 16QAM signal. (a) BER curves versus input power launched into PD; (b) the recovered constellation in 1-m wireless transmission case using DSP technology at 1.5-dBm input power: (b)-i after resampling; (b)-ii after CMA; (b)-iii after FOE; (b)-iv after POE; (c) the constellation diagram after the decision-directed least mean square algorithm (DDLMS).

of five points are measured in each situation until the power of PD is increased to 1.5 dBm. When the input power is over 0 dBm, the measured BER can go below the HD-FEC threshold. Fig. 9(b) illustrates the recovered constellation after DSP techniques including resampling, CMA, FOE and POE. From Fig. 9(b)–i to Fig. 9(b)–iv, the constellation changes from a blurring pie into 16QAM constellation points. And after the decision-directed least mean square algorithm (DDLMS), the constellation diagram becomes much clearer, as shown in Fig. 9(c). The BER performance for 130-GHz mm-wave 4-Gbaud 16QAM transmission is measured as shown in Fig. 10. We compare

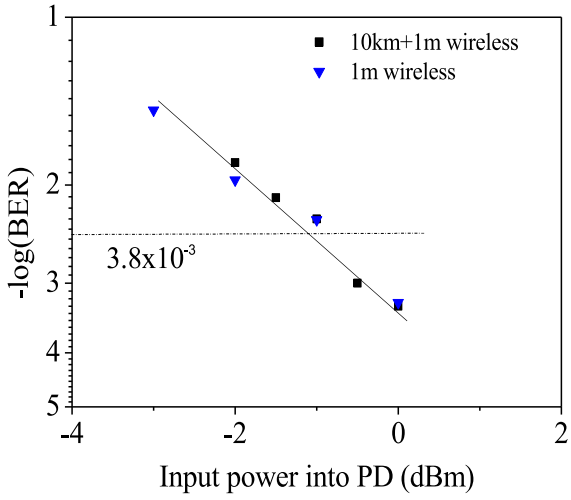

Fig. 10. BER curves versus input power launched into PD for 130-GHz 4-Gbaud 16QAM signal.

the BER curves for the 130-GHz, 4-Gbaud 16QAM signal in the ROF scheme over 1-m wireless and 10-km SMF transmission with that of only 1-m wireless link system. In the two cases, the BER performances are similar. As the input power into PD increases, the BER curves performs better. The HD-FEC threshold can be reached when the input power is increased to -1 dBm, which shows better BER performance than 150-GHz mm-wave 4-Gbaud 16QAM transmission.

4. Conclusion

We proposed a novel system for D-band mm-wave SSB vector signal generation based on two intensity modulators including one single-drive MZM driven by a 20-GHz RF signal and one push-pull MZM driven by a 4-Gbaud signal at the 10-GHz central frequency. Using the first MZM, an optical frequency comb including six odd-order flattop carriers with a frequency spacing of 20-GHz can be successfully obtained. By using the subsequent push-pull MZM, SSB vector signals are generated. Based on this scheme, we experimentally generated D-band SSB vector signals at the frequencies of 130-GHz and 150-GHz using two selected sidebands, respectively. In addition, 4-Gbaud QPSK and 16QAM signals were transmitted in a ROF link over 10-km/25-km SMF and 1-m wireless distance. The results demonstrated that the proposed system can realize wireless data transmission with a BER less than 3.8×10^{-3} over 10-km/25-km single-mode-fiber (SMF) and 1-m wireless links. This D-band mm-wave generation technology greatly increases the flexibility of mm-wave frequencies generation and reduces the transmitter complexity, which can be widely used in 5th-generation (5G) and the next-generation communication.

References

[1] X. Li, J. Yu, and G. K. Chang, "Photonics-assisted technologies for extreme broadband 5G wireless communications," *J. Lightw. Technol.*, vol. 37, no. 12, pp. 2851–2865, Jun. 2019.
[2] L. Zhang *et al.*, "Generation and transmission of multiband and multi-gigabit 60-GHz MMW signals in an RoF system with frequency quintupling technique," *Opt. Express*, vol. 21, no. 8, pp. 9899–9905, 2013.
[3] K. Kitayama, A. Maruta, and Y. Yoshida, "Digital coherent technology for optical fiber and radio-over-fiber transmission systems," *J. Lightw. Technol.*, vol. 32, no. 20, pp. 3411–3420, Oct. 2014.
[4] M. J. Fice *et al.*, "146-GHz millimeter-wave radio-over-fiber photonic wireless transmission system," *Opt. Express*, vol. 20, no. 2, pp. 1769–1774, 2012.
[5] L. Zhao, J. G. Yu, L. Chen, P. Min, J. Li, and R. Wang, "16QAM vector millimeter-wave signal generation based on phase modulator with photonic frequency doubling and precoding," *IEEE Photon. J.*, vol. 8, no. 2, Apr. 2016, Art. no. 5500708.
[6] X. Li, Y. Xu, and J. Yu, "Single-sideband W-band photonic vector millimeter-wave signal generation by one single I/Q modulator," *Opt. Lett.*, vol. 41, no. 18, pp. 4162–4165, 2016.

[7] H. T. Huang *et al.*, "High spectral efficient W-band OFDM-RoF system with direct-detection by two cascaded single-drive MZMs," *Opt. Express*, vol. 21, no. 14, pp. 16615–16620, 2013.
[8] J. Yu, Z. Jia, L. Yi, Y. Su, G. K. Chang, and T. Wang, "Optical millimeter-wave generation or up-conversion using external modulators," *IEEE Photon. Technol. Lett.*, vol. 18, no. 1, pp. 265–267, Jan. 2006.
[9] X. Li, J. Zhang, J. Xiao, Z. Zhang, Y. Xu, and J. Yu, "W-Band 8QAM vector signal generation by MZM-based photonic frequency octupling," *IEEE Photon. Technol. Lett.*, vol. 27, no. 12, pp. 1257–1260, Jun. 2015.
[10] X. Li, Y. Xu, J. Xiao, and J. Yu, "W-band millimeter-wave vector signal generation based on precoding-assisted random photonic frequency tripling scheme enabled by phase modulator," *IEEE Photon. J.*, vol. 8, no. 2, Apr. 2016, Art. no. 5500410.
[11] X. Li, J. Yu, Z. Zhang, J. Xiao, and G. K. Chang, "Photonic vector signal generation at W-band employing an optical frequency octupling scheme enabled by a single MZM," *Opt. Commun.*, vol. 349, pp. 6–10, 2015.
[12] L. Chen, R. Deng, J. He, Q. Chen, Y. Liu, and C. Xing, "W-band vector signal generation by photonic frequency quadrupling and balanced pre-coding," *IEEE Photon. Technol. Lett*, vol. 28, no. 17, pp. 1807–1810, Sep. 2016.
[13] X. Li and J. Yu, "Over 100 Gb/s ultrabroadband MIMO wireless signal delivery system at the D-band," *IEEE Photon. J.*, vol. 8, no. 5, pp. 1–10, Oct. 2016.
[14] M. L. Frecassetti *et al.*, "D-band radio solutions for beyond 5G reconfigurable meshed cellular networks," in *Int. Symp. Wireless Commun. Syst.*, 2019.
[15] X. Li, Y. Xu, J. Xiao, and J. Yu, "A 2 $\times$ 2 MIMO optical wireless system at D-band," in *Proc. Opt. Fiber Commun. Conf. Exhib.*, 2016.
[16] C. T. Lin *et al.*, "Optical direct-detection OFDM signal generation for radio-over-fiber link using frequency doubling scheme with carrier suppression," *Opt. Express*, vol. 16, no. 9, pp. 6056–6063, 2008.
[17] H. Zhang, L. Cai, S. Xie, K. Zhang, X. Wu, and Z. Dong, "A novel radio-over-fiber system based on carrier suppressed frequency eightfold millimeter wave generation," *IEEE Photon. J.*, vol. 9, no. 5, pp. 1–6, Oct. 2017.
[18] W. Xu *et al.*, "High spectral purity millimeter wave generation and wavelength reuse radio over fiber system based on modified double sideband," in *Proc. Wireless Opt. Commun. Conf.*, 2016.
[19] Y. Xu, X. Li, J. Yu, and G. K. Chang, "Simple and reconfigured single-sideband OFDM RoF system," *Opt. Express*, vol. 24, no. 20, pp. 22830–22835, 2016.
[20] Wen Zhou, Li Zhao, Jiao Zhang, and Kaihui Wang, "Four sub-channel single sideband generation of vector mm-wave based on an I/Q modulator," *IEEE Photon. J.*, vol. 11, no. 4, Aug. 2019, Art. no. 7204409.
[21] L. Zhang *et al.*, "C-band single wavelength 100-Gb/s IM-DD transmission over 80-km SMF without CD compensa*tion using SSB-DMT*," in *Proc. IEEE Optical Fiber Commun. Conf.*, 2015.
[22] M. Niknamfar and M. Shadaram, "Two cascaded Mach-Zehnder modulators' harmonic distortion analysis in single side-band millimeter wave generation system," in *Int. Conf. Transp. Opt. Networks*, 2015.
[23] W. Zhou, X. Li, and J. Yu, "Pre-coding assisted generation of a frequency quadrupled optical vector D-band millimeter wave with one Mach-Zehnder modulator," *Opt. Express*, vol. 25, no. 22, pp. 26483–26491, 2017.
[24] X. Li, "Optimization of precoding phase distribution for frequency-multiplication vector signal generation," *IEEE Photon. J.*, vol. 9, no. 3, Jun. 2017, Art. no. 5502207.
[25] A. Narasimha, X. Meng, M. Wu, and E. Yablonovitch, "Tandem single sideband modulation scheme for doubling spectral efficiency of analogue fibre links," *Electron. Lett.*, vol. 36, no. 13, pp. 1135–1136, 2000.
[26] P. Saghari, S. Nezam, A. Sahin, and A. Willner, "Polarization-state-rotation and filtering receiver for bandwidth- efficient tandem single sideband systems," in *Proc. Opt. Fiber Commun. Conf.*, 2004.
[27] J. Zhang *et al.*, "Simplified coherent receiver with heterodyne detection of eight-channel 50 Gb/s PDM-QPSK WDM signal after 1040 km SMF-28 transmission," *Opt. Lett.*, vol. 37, no. 19, pp. 4050–4052, 2012.
[28] J. Yu and X. Zhou, "Ultra-high-capacity DWDM transmission system for 100G and beyond," *IEEE Commun. Mag.*, vol. 48, no. 3, pp. S56–S64, Mar. 2010.
[29] J Yu, X Li, and W Zhou, "Tutorial: Broadband fiber-wireless integration for 5G+ communication," *APL Photon.*, vol. 3, no. 11, 2018, Art. no. 111101.
[30] J. Yu, "Photonics-assisted millimeter-wave wireless communication." *IEEE J. Quantum Electron.*, vol. 53, no. 6, pp. 1–17, Dec. 2017.
[31] X. Li, J. Xiao, and J. Yu, "Long-distance wireless mm-wave signal delivery at W-band," *J. Lightw. Technol.*, vol. 34, no. 2, pp. 661–668, Jan.2016.